





Transit Light Curves for Exomoons: Analytical Formalism

Suman Saha^{1,2}  and Sujan Sengupta¹ ¹ Indian Institute of Astrophysics, II Block, Koramangala, Bengaluru, India; suman.saha@iiap.res.in² Pondicherry University, R.V. Nagar, Kalapet, Puducherry, India

Received 2021 November 29; revised 2022 July 28; accepted 2022 July 30; published 2022 August 25

Abstract

The photometric transit method has been the most effective method to detect and characterize exoplanets as several ground based as well as space based survey missions have discovered thousands of exoplanets using this method. With the advent of the upcoming next generation large telescopes, the detection of exomoons in a few of these exoplanetary systems is very plausible. In this paper, we present a comprehensive analytical formalism in order to model the transit light curves for such moon-hosting exoplanets. In order to achieve analytical formalism, we have considered circular orbit of the exomoon around the host planet, which is indeed the case for tidally locked moons. The formalism uses the radius and orbital properties of both the host planet and its moon as model parameters. The coalignment or noncoalignment of the orbits of the planet and the moon are parameterized using two angular parameters and thus can be used to model all the possible orbital alignments for a star–planet–moon system. This formalism also provides unique and direct solutions to every possible star–planet–moon three circular body alignment. Using the formula derived, a few representative light curves are also presented.

Unified Astronomy Thesaurus concepts: Exoplanets (498); Natural satellites (Extrasolar) (483); Transit photometry (1709)

1. Introduction

The large number of natural satellites around the planets in our solar system suggests a high possibility of the existence of such subplanetary bodies around many of the exoplanets discovered to date. In the past two decades, more than 4000 exoplanets with a wide range of size and mass have been discovered by using various detection techniques. However, the discovery of natural satellites (also known as exomoons) in those systems still remains elusive.

Out of the various detection techniques used for the discovery of exoplanets, the transit method has been proven to be the most effective. Apart from detection, the transit method also provides a way to estimate the size and orbital properties of the exoplanets accurately. Derivatives of the transit method involving the effect of the exomoon on the companion exoplanet, such as the transit-timing variation (TTV, Sartoretti & Schneider 1999; Szabó et al. 2006), and the transit-duration variation (Kipping 2009) have been proposed for the detection of exomoons. However, the amplitude of these effects is extremely small for sub-Earth mass exomoons and so far no confirmed exomoon candidate has been detected using these techniques (Fox & Wiegert 2021; Kipping 2020, 2021). Several other techniques have also been proposed for the detection of exomoons, such as photometric orbital sampling effect (Heller 2014; Teachey et al. 2018), imaging of mutual transits (Cabrera & Schneider 2007), microlensing (Han & Han 2002), spectroscopy (Williams & Knacke 2004; Johnson & Huggins 2006; Oza et al. 2019), polarimetry of self-luminous exoplanets (Sengupta & Marley 2016), Doppler monitoring of direct images of exoplanets (Agol et al. 2015), pulsar timing (Lewis et al. 2008), and radio emissions of giant exoplanets (Noyola et al. 2014, 2016). However, no confirmed

exomoon candidate has yet been detected by using any of these techniques.

A shortcoming of the transit method is that the transit probability decreases with the increase in the orbital distance of the exoplanets from their host stars. Also, with the increase in the orbital distance, the orbital period of the exoplanets increases reducing the probability of detection as it requires continuous monitoring for a longer time period to confirm the detection. Both these factors have severely constrained the discovery of exoplanets in wider orbits. Previous studies (Namouni 2010; Spalding et al. 2016; Dobos et al. 2021) have shown that the exoplanets in close-in orbits are likely to lose any natural satellites during the orbital migration. This could be the prime reason behind the lack of discovery of exomoons around the planetary systems discovered to date. With the installation of dedicated survey telescopes, both ground based and space based, and a combination of the observations from multiple observing facilities, the detection of exoplanets in wider orbits in near future is enabled. Such facilities may also enable the detection of natural satellites around the exoplanets.

Another major factor that makes it difficult to detect the exomoons through the photometric transit method is the requirement of extreme precision. Survey missions like the CoRoT, Kepler, and TESS, and the 2 m class Hubble Space Telescope have made it possible to detect and study exoplanets as small as the Earth. However, the detection probability of such smaller exoplanets is more around the smaller late-K or M-dwarf stars compared to the larger stars of similar apparent magnitude. This is because the precision required to detect exoplanets is proportional to the ratio of disk area of the planet to the star. On the other hand, the largest of the natural satellites in our solar system has a radius even smaller than half of the radius of the Earth. Such smaller natural satellites may be abundant in many exoplanetary systems, but their detection would require a much better photometric precision. All these factors sum up to the inference that the detection of exomoons would require a precision higher than that achievable using the



Original content from this work may be used under the terms of the [Creative Commons Attribution 4.0 licence](https://creativecommons.org/licenses/by/4.0/). Any further distribution of this work must maintain attribution to the author(s) and the title of the work, journal citation and DOI.

currently available instruments. However, the next generation of large telescopes, such as the James Webb Space Telescope (JWST), the European Extremely Large Telescope (E-ELT), the Thirty Meter Telescope (TMT), and the Giant Magellan Telescope (GMT), etc., will make it possible to achieve such extremely high precision. Also, the major improvements in small-scale noise reduction techniques (Johnson et al. 2015; Livingston et al. 2019; Chakrabarty & Sengupta 2019; Saha et al. 2021; Saha & Sengupta 2021) will help in such studies to improve the precision of photometric light curves.

As a consequence, it is very much likely that the improved facilities in the near future will make it possible to detect the exomoons through the photometric transit method. In that case, a self-consistent and mathematically straightforward analytical formalism will be necessary to model the transit light curves of stars having moon-hosting planets and to estimate the physical properties of the exomoons. The theoretical models need also to be unambiguous enough to be applicable for all possible realistic scenarios of the position of the exomoon with respect to the host exoplanet, and will thus help to strategize the observational parameters to such extremely time-critical observations. We therefore, present in this paper a comprehensive and generic analytical formalism for the light curves of a transiting exoplanetary system with an exomoon in terms of the radius and orbital parameters of both the planet and the moon. An important aspect of such formalism is to formulate the motion of the three bodies in a common reference frame with respect to the observer. The existing formalism (Kipping 2011; Teachey & Kipping 2018) relies on the rotational transformation of the individual orbits for this purpose. On the other hand, we present a comparatively simple and straightforward analytical formalism by taking into account only the physically significant orbital parameters of the exoplanet and a circularly orbiting exomoon, such that one can easily model the transit light curves for every possible orbital alignment of the system. To account for the independent spatial inclination of the orbits of the planet and the moon in a simpler way, we have used a two angular parameter approach. We have also provided direct and straightforward solutions to the conditions for various alignments of the star–planet–moon system, especially for the cases where all the three circular bodies intersect with each other. In Section 2, we discuss the analytical formalism, in Section 3, we present the results, and in Section 4, we conclude our study.

2. Analytical Formalism

Let us consider a natural satellite or moon with radius r_m , orbiting a planet with radius r_p , where r_m and r_p are expressed in term of the radius of the star. If the moon is sufficiently massive, the barycenter of the planet–moon system will be significantly away from the center of the planet even though it lies inside the planetary surface. However, the barycenter will follow the same orbit as the planet would in the absence of a moon. In order to achieve a simple analytical formalism, we have considered a circular orbit for the barycenter around the star. This provides us the advantage of the underlying symmetry. For most of the cases, the orbital eccentricity of an exoplanet can only be estimated by using the radial-velocity method, and a prior knowledge of it would be required to model the transit light curve correctly. However, in the absence of a prior information of the eccentricity, modeling the transit signal for a circular orbit would result in a slightly different

value for the orbital semimajor axis and the orbital inclination of the planet. However, it would not affect the orbital properties of the moon.

In the formalism presented here, we have used subscripts s , p , m , and b to denote the star, the planet, the moon, and the planet–moon barycenter, respectively. Now, the separation of the barycenter of the planet–moon system from the center of the star is given by

$$z_{sb} = a_b \sqrt{\sin^2 \theta_b + \cos^2 \theta_b \cos^2 i_b} \quad (1)$$

$$\theta_b = \frac{2\pi}{P_b}(t - t_{0b}), \quad (2)$$

where a_b is the semimajor axis, i_b is the inclination angle, θ_b is the orbital phase, P_b is the orbital period, and t_{0b} is the midtransit time of the planet–moon barycenter around the star.

If we consider the distance between centers of the moon and the planet to be r_{pm} , the distance of the center of the moon from the planet–moon barycenter is $a_m = r_{pm}/(1 + M_m/M_p)$, where M_m is the mass of the moon and M_p is the mass of the planet, and the distance of the center of the planet from the planet–moon barycenter is $a_p = r_{pm} - a_m$. Now, the separation between the center of the moon and the barycenter of the planet–moon system is given by

$$z_{mb} = a_m \sqrt{\sin^2 \theta_m + \cos^2 \theta_m \cos^2 i_m} \quad (3)$$

$$\theta_m = \frac{2\pi}{P_m}(t - t_{0m}) \quad (4)$$

and the separation of the center of the planet from the barycenter of the planet–moon system can be written as

$$z_{pb} = a_p \sqrt{\sin^2 \theta_m + \cos^2 \theta_m \cos^2 i_m}, \quad (5)$$

where a_m is the semimajor axis of the moon, a_p is the semimajor axis of the planet, i_m is the inclination angle, θ_m is the orbital phase, P_m is the orbital period, and t_{0m} is the midtransit time of the moon around the planet–moon barycenter. Note that, the orbital inclination angle of the moon is also measured with respect to the point of view of the observer. The separation between the center of the planet and the center of the moon is

$$z_{pm} = z_{mb} + z_{pb}. \quad (6)$$

We denote the angle between the major axes of the projected orbits of the planet–moon barycenter around the star and the moon around the planet–moon barycenter as α_{mb} (see Figure 1). Now, the separation between the centers of the planet and the star can be written as

$$z_{sp} = \sqrt{z_{sb}^2 + z_{pb}^2 - 2z_{sb}z_{pb} \cos \phi} \quad (7)$$

$$\phi = \alpha_{mb} + \eta - \eta_1 \quad (8)$$

$$\eta = \begin{cases} \cos^{-1} \frac{\cos \theta_b \cos i_b}{\sqrt{\sin^2 \theta_b + \cos^2 \theta_b \cos^2 i_b}}, & 0 \leq \theta_b \leq \pi \\ -\cos^{-1} \frac{\cos \theta_b \cos i_b}{\sqrt{\sin^2 \theta_b + \cos^2 \theta_b \cos^2 i_b}}, & -\pi \leq \theta_b < 0 \end{cases} \quad (9)$$

$$\eta_1 = \begin{cases} \cos^{-1} \frac{\cos \theta_m \cos i_m}{\sqrt{\sin^2 \theta_m + \cos^2 \theta_m \cos^2 i_m}}, & 0 \leq \theta_m \leq \pi \\ -\cos^{-1} \frac{\cos \theta_m \cos i_m}{\sqrt{\sin^2 \theta_m + \cos^2 \theta_m \cos^2 i_m}}, & -\pi \leq \theta_m < 0, \end{cases} \quad (10)$$

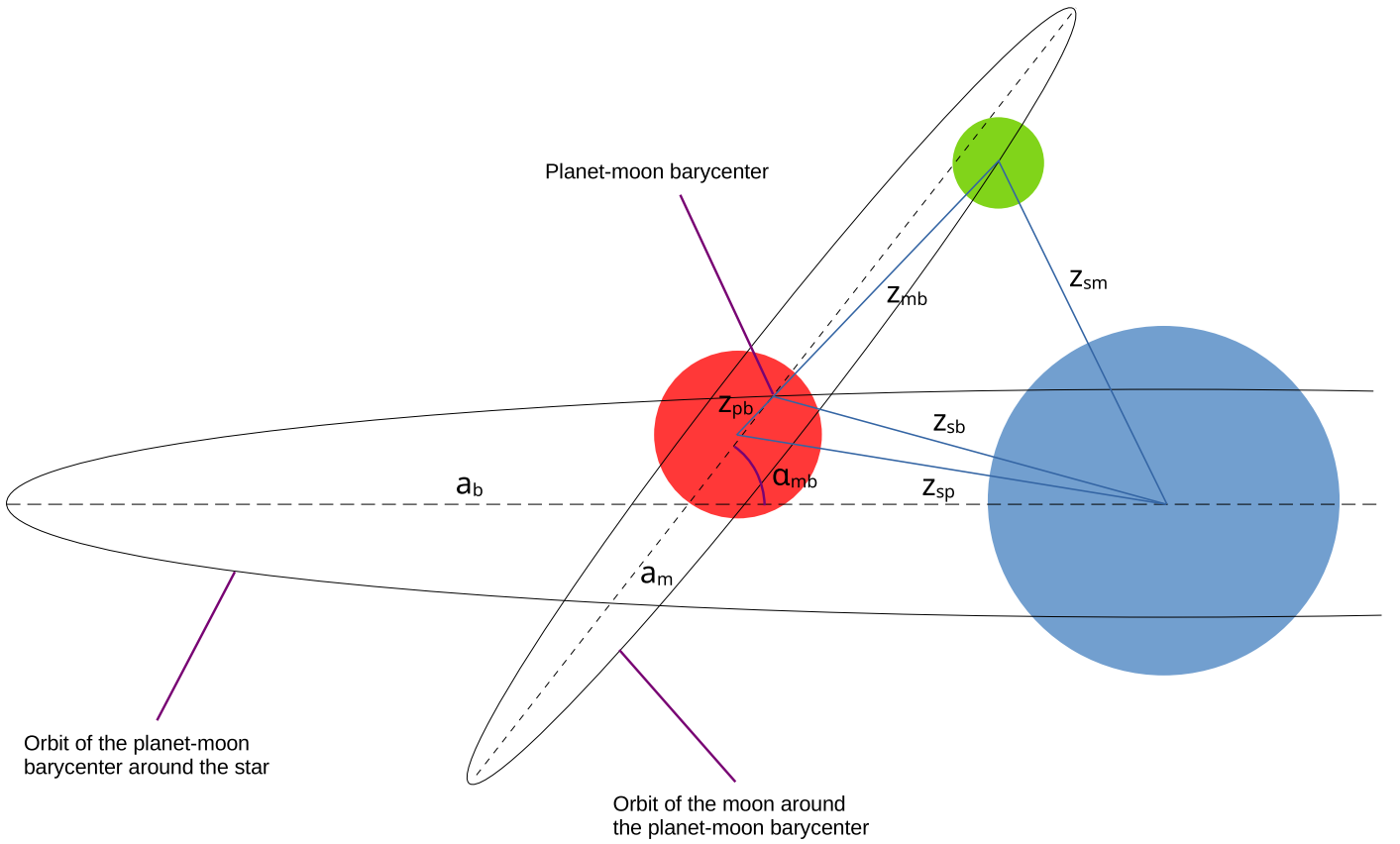


Figure 1. Orbital orientation of the star–planet–moon system from the observer’s point of view, showing z_{sp} , z_{pm} , and z_{sm} , the separations between the centers of the star and the planet, the planet, and the moon, and the star and the moon, respectively; z_{sb} , z_{pb} , and z_{mb} , the separation of the planet–moon barycenter from the centers of the star, the planet, and the moon, respectively; α_{mb} , the angle between the major axes of the projected orbits of the planet–moon barycenter around the star and the moon around the planet–moon barycenter; a_b and a_m , the orbital semimajor axes of the planet–moon barycenter around the star and the moon around the planet–moon barycenter, respectively.

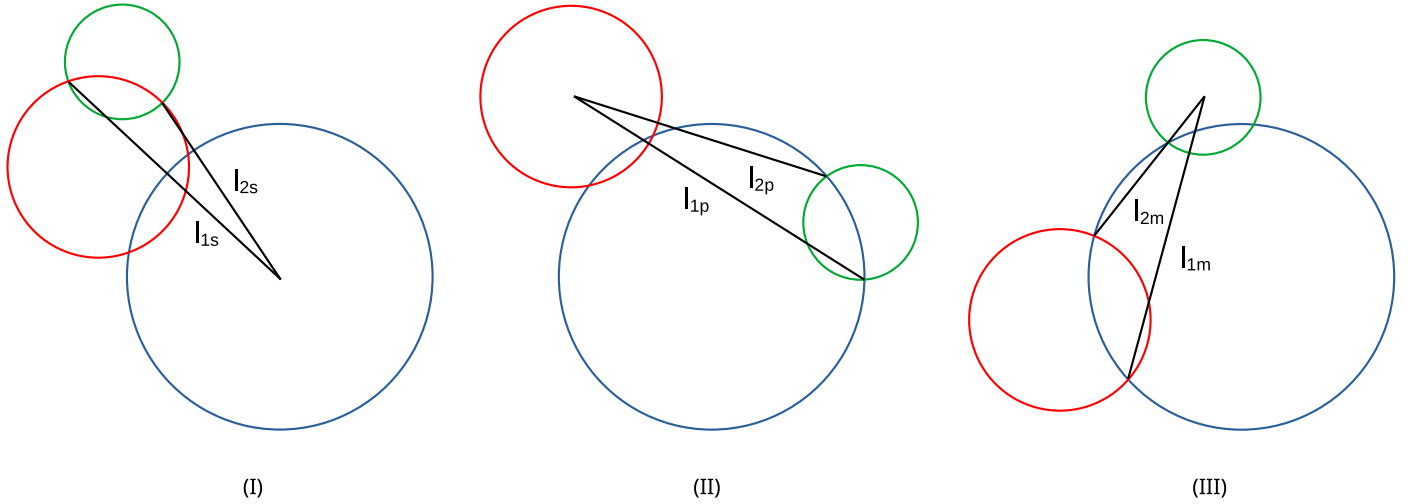


Figure 2. (I) Alignment with star–planet and planet–moon intersections showing l_{1s} and l_{2s} , the separation of the star from the points of intersection of the planet and the moon; (II) alignment with star–planet and star–moon intersections showing l_{1p} and l_{2p} , the separation of the planet from the points of intersection of the star and the moon; (III) alignment with star–planet and star–moon intersections showing l_{1m} and l_{2m} , the separation of the moon from the points of intersection of the star and the planet.

where ϕ is the angle between z_{sb} and z_{pb} . Similarly, the separation between the centers of the moon and the star is written as

$$z_{sm} = \sqrt{z_{sb}^2 + z_{mb}^2 - 2z_{sb}z_{mb} \cos \phi_1} \quad (11)$$

$$\phi_1 = \pi - \phi. \quad (12)$$

If the ratio between the mass of the moon and the planet is assumed very small, the barycenter of the planet–moon system could be approximated at the center of the planet, i.e., $a_p = 0$, in which case the model simplifies to $z_{pb} = 0$, $z_{sp} = z_{sb}$, and $z_{pm} = z_{mb}$.

The separation of the star from the points of intersection of the moon and the planet (see Figure 2 and Appendix) are given by

$$l_{1s} = \sqrt{r_p^2 + z_{sp}^2 - 2r_p z_{sp} \cos \left(\cos^{-1} \frac{z_{sp}^2 + z_{pm}^2 - z_{sm}^2}{2z_{sp}z_{pm}} + \cos^{-1} \frac{r_p^2 - r_m^2 + z_{pm}^2}{2z_{pm}r_p} \right)} \quad (13)$$

$$l_{2s} = \sqrt{r_p^2 + z_{sp}^2 - 2r_p z_{sp} \cos \left(\cos^{-1} \frac{z_{sp}^2 + z_{pm}^2 - z_{sm}^2}{2z_{sp}z_{pm}} - \cos^{-1} \frac{r_p^2 - r_m^2 + z_{pm}^2}{2z_{pm}r_p} \right)}. \quad (14)$$

Similarly, the separation of the planet from the points of intersection of the moon and the star are given by

$$l_{1p} = \sqrt{r_m^2 + z_{pm}^2 - 2r_m z_{pm} \cos \left(\cos^{-1} \frac{z_{pm}^2 + z_{sm}^2 - z_{sp}^2}{2z_{pm}z_{sm}} + \cos^{-1} \frac{r_m^2 - 1 + z_{sm}^2}{2z_{sm}r_m} \right)} \quad (15)$$

$$l_{2p} = \sqrt{r_m^2 + z_{pm}^2 - 2r_m z_{pm} \cos \left(\cos^{-1} \frac{z_{pm}^2 + z_{sm}^2 - z_{sp}^2}{2z_{pm}z_{sm}} - \cos^{-1} \frac{r_m^2 - 1 + z_{sm}^2}{2z_{sm}r_m} \right)}. \quad (16)$$

Also, the separation of the moon from the points of intersection of the star and the planet are given by

$$l_{1m} = \sqrt{r_p^2 + z_{pm}^2 - 2r_p z_{pm} \cos \left(\cos^{-1} \frac{z_{pm}^2 + z_{sp}^2 - z_{sm}^2}{2z_{pm}z_{sp}} + \cos^{-1} \frac{r_p^2 - 1 + z_{sp}^2}{2z_{sp}r_p} \right)} \quad (17)$$

$$l_{2m} = \sqrt{r_p^2 + z_{pm}^2 - 2r_p z_{pm} \cos \left(\cos^{-1} \frac{z_{pm}^2 + z_{sp}^2 - z_{sm}^2}{2z_{pm}z_{sp}} - \cos^{-1} \frac{r_p^2 - 1 + z_{sp}^2}{2z_{sp}r_p} \right)}. \quad (18)$$

The normalized flux from the star is given by

$$F = 1 - \frac{F'}{F_T}, \quad (19)$$

where F_T is the unobscured flux of the star, and F' is the occulted flux. If F'_p is the flux occulted by the planet and F'_m is that by the moon, then

$$F' = F'_p + F'_m. \quad (20)$$

Under small-planet approximation, i.e., $r_p, r_m \lesssim 0.1$, we have followed the prescription by Mandel & Agol (2002). Hence, we have

$$F'_p = \frac{2A_{op}}{(\rho_{2p}^2 - \rho_{1p}^2)} \int_{\rho_{1p}}^{\rho_{2p}} I(\rho) \rho d\rho \quad (21)$$

$$F'_m = \frac{2A_{om}}{(\rho_{2m}^2 - \rho_{1m}^2)} \int_{\rho_{1m}}^{\rho_{2m}} I(\rho) \rho d\rho \quad (22)$$

$$(\rho_{1p}, \rho_{2p}) = \begin{cases} (0, z_{sp} + r_p), & z_{sp} \leq r_p, \\ (z_{sp} - r_p, z_{sp} + r_p), & r_p < z_{sp} < 1 - r_p, \\ (z_{sp} - r_p, 1), & 1 - r_p \leq z_{sp} < 1 + r_p \end{cases} \quad (23)$$

$$(\rho_{1m}, \rho_{2m}) = \begin{cases} (0, z_{sm} + r_m), & z_{sm} \leq r_m, \\ (z_{sm} - r_m, z_{sm} + r_m), & r_m < z_{sm} < 1 - r_m, \\ (z_{sm} - r_m, 1), & 1 - r_m \leq z_{sm} < 1 + r_m, \end{cases} \quad (24)$$

where $I(\rho)$ is the specific intensity, ρ being the radial distance, A_{op} is the area of the stellar disk occulted by the planet, and A_{om} is that occulted by the moon.

Thus, the normalized flux from the star can be written as

$$F = 1 - \frac{2}{F_T} \left[\frac{A_{op}}{(\rho_{2p}^2 - \rho_{1p}^2)} \int_{\rho_{1p}}^{\rho_{2p}} I(\rho) \rho d\rho + \frac{A_{om}}{(\rho_{2m}^2 - \rho_{1m}^2)} \int_{\rho_{1m}}^{\rho_{2m}} I(\rho) \rho d\rho \right]. \quad (25)$$

Different alignments of the star, the planet, and the moon result into different values of A_{op} and A_{om} . We have categorized all the possible alignments into 22 cases, as shown in Figure 3. Similar categorizations were previously provided by Fewell (2006) and Kipping (2011). However, we have made a more concise categorization considering only the physically feasible alignments and a

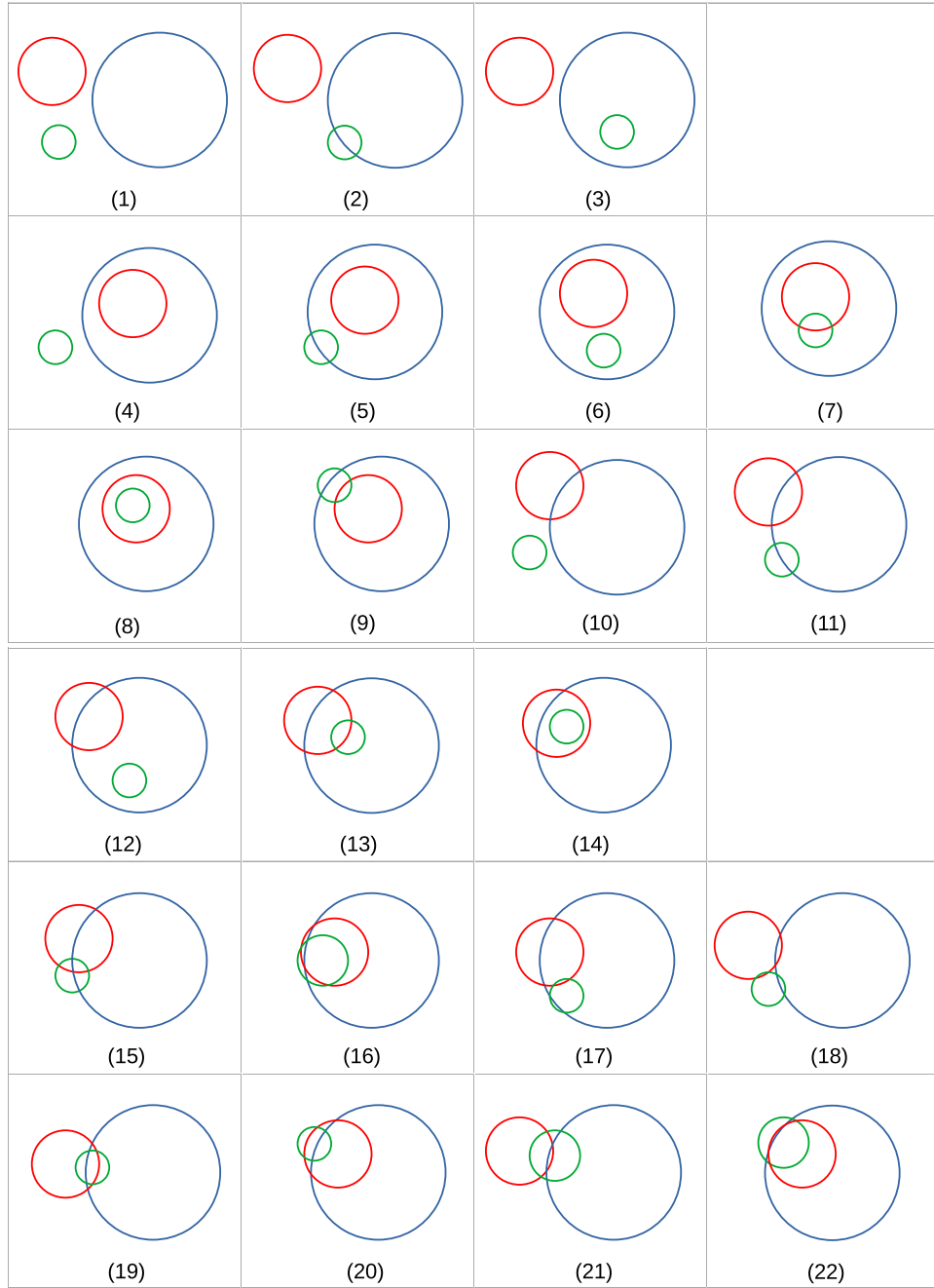


Figure 3. An instance of all possible cases of alignment for the star (blue), the planet (red), and the moon (green).

more straightforward criteria for where they hold. The conditions where these cases hold, along with the values of A_{op} and A_{om} are listed in Table 1. Various terms for the area used in Table 1 are as follows.

$A_p = \pi r_p^2$ and $A_m = \pi r_m^2$ are the disk areas of the planet and the moon, respectively; A_{sp} , A_{pm} , and A_{sm} are the areas of intersections of star–planet, planet–moon, and star–moon, respectively (Mandel & Agol 2002), given by

$$A_{\text{sp}} = \cos^{-1} \frac{1 - r_p^2 + z_{\text{sp}}^2}{2z_{\text{sp}}} + r_p^2 \cos^{-1} \frac{r_p^2 - 1 + z_{\text{sp}}^2}{2z_{\text{sp}}r_p} - \sqrt{z_{\text{sp}}^2 - \frac{(1 - r_p^2 + z_{\text{sp}}^2)^2}{4}} \quad (26)$$

$$A_{\text{pm}} = r_p^2 \cos^{-1} \frac{r_p^2 - r_m^2 + z_{\text{pm}}^2}{2z_{\text{pm}}r_p} + r_m^2 \cos^{-1} \frac{r_m^2 - r_p^2 + z_{\text{pm}}^2}{2z_{\text{pm}}r_m} - \sqrt{z_{\text{pm}}^2 r_p^2 - \frac{(r_p^2 - r_m^2 + z_{\text{pm}}^2)^2}{4}} \quad (27)$$

$$A_{\text{sm}} = \cos^{-1} \frac{1 - r_m^2 + z_{\text{sm}}^2}{2z_{\text{sm}}} + r_m^2 \cos^{-1} \frac{r_m^2 - 1 + z_{\text{sm}}^2}{2z_{\text{sm}}r_m} - \sqrt{z_{\text{sm}}^2 - \frac{(1 - r_m^2 + z_{\text{sm}}^2)^2}{4}} \quad (28)$$

Following a similar formalism as given by Fewell (2006), the area of intersection of all the three bodies, i.e., the star, the

Table 1
Different Cases of Star–Planet–Moon Alignments

Case	Conditions	A_{op}	A_{om}
1	$z_{\text{sp}} \geq 1 + r_p$ $z_{\text{sm}} \geq 1 + r_m$	0	0
2	$z_{\text{sp}} \geq 1 + r_p$ $1 + r_m > z_{\text{sm}} > 1 - r_m$	0	A_{sm}
3	$z_{\text{sp}} \geq 1 + r_p$ $z_{\text{sm}} \leq 1 - r_m$	0	A_{pm}
4	$z_{\text{sp}} \leq 1 - r_p$ $z_{\text{pm}} \geq r_p + r_m$ $z_{\text{sm}} \geq 1 + r_m$	A_p	0
5	$z_{\text{sp}} \leq 1 - r_p$ $z_{\text{pm}} \geq r_p + r_m$ $1 + r_m > z_{\text{sm}} > 1 - r_m$	A_p	A_{sm}
6	$z_{\text{sp}} \leq 1 - r_p$ $z_{\text{pm}} \geq r_p + r_m$ $z_{\text{sm}} \leq 1 - r_m$	A_p	A_m
7	$z_{\text{sp}} \leq 1 - r_p$ $r_p + r_m > z_{\text{pm}} > r_p - r_m$ $z_{\text{sm}} \leq 1 - r_m$	A_p	$A_m - A_{\text{pm}}$
8	$z_{\text{sp}} \leq 1 - r_p$ $z_{\text{pm}} \leq r_p - r_m$ $z_{\text{sm}} \leq 1 - r_m$	A_p	0
9	$z_p \leq 1 - r_{\text{sp}}$ $r_p + r_m > z_{\text{pm}} > r_p - r_m$ $1 + r_m > z_{\text{sm}} > 1 - r_m$	A_p	$A_{\text{sm}} - A_{\text{pm}}$
10	$1 + r_p > z_{\text{sp}} > 1 - r_p$ $z_{\text{sm}} \geq 1 + r_m$	A_{sp}	0
11	$1 + r_p > z_{\text{sp}} > 1 - r_{\text{sp}}$ $z_m \geq r_p + r_m$ $1 + r_m > z_{\text{sm}} > 1 - r_m$	A_{sp}	A_{sm}
12	$1 + r_p > z_{\text{sp}} > 1 - r_p$ $z_{\text{pm}} \geq r_p + r_m$ $z_{\text{sm}} \leq 1 - r_m$	A_{sp}	A_m
13	$1 + r_p > z_{\text{sp}} > 1 - r_p$ $r_p + r_m > z_{\text{pm}} > r_p - r_m$ $z_{\text{sm}} \leq 1 - r_m$	A_{sp}	$A_m - A_{\text{pm}}$
14	$1 + r_p > z_{\text{sp}} > 1 - r_p$ $z_{\text{pm}} \leq r_p - r_m$	A_{sp}	0
15	$1 + r_p > z_{\text{pm}} > 1 - r_p$ $r_p + r_m > z_{\text{pm}} > r_p - r_m$ $1 + r_m > z_{\text{sm}} > 1 - r_m$ $l_{1m} > r_m > l_{2m}$ $D \geq 0$	A_{sp}	$A_{\text{sm}} - A_{\text{spm1}}$
16	$1 + r_p > z_{\text{sp}} > 1 - r_p$ $r_p + r_m > z_{\text{pm}} > r_p - r_m$ $1 + r_m > z_{\text{sm}} > 1 - r_m$ $l_{1m} > r_m > l_{2m}$ $D < 0$	A_{sp}	$A_{\text{sm}} - A_{\text{spm2}}$
17	$1 + r_p > z_{\text{sp}} > 1 - r_p$ $r_p + r_m > z_{\text{pm}} > r_p - r_m$ $1 + r_m > z_{\text{sm}} > 1 - r_m$ $1 \geq l_{1s} \geq l_{2s}$ $l_{1p} \geq l_{2p} \geq r_p$ $l_{1m} \geq l_{2m} \geq r_m$	A_{sp}	$A_{\text{sm}} - A_{\text{pm}}$

Table 1
(Continued)

Case	Conditions	A_{op}	A_{om}
18	$1 + r_p > z_{\text{pm}} > 1 - r_p$ $r_p + r_m > z_{\text{pm}} > r_p - r_m$ $1 + r_m > z_{\text{sm}} > 1 - r_m$ $l_{1s} \geq l_{2s} \geq 1$ $l_{1p} \geq l_{2p} \geq r_p$ $l_{1m} \geq l_{2m} \geq r_m$	A_{sp}	A_{sm}
19	$1 + r_p > z_{\text{sp}} > 1 - r_p$ $r_p + r_m > z_{\text{pm}} > r_p - r_m$ $1 + r_m > z_{\text{sm}} > 1 - r_m$ $1 \geq l_{1s} \geq l_{2s}$ $r_p \geq l_{1p} \geq l_{2p}$ $l_{1m} \geq l_{2m} \geq r_m$	A_{sp}	$A_m - A_{\text{pm}}$
20	$1 + r_p > z_{\text{sp}} > 1 - r_p$ $r_p + r_m > z_{\text{pm}} > r_p - r_m$ $1 + r_m > z_{\text{sm}} > 1 - r_m$ $l_{1s} \geq l_{2s} \geq 1$ $r_p \geq l_{1p} \geq l_{2p}$ $l_{1m} \geq l_{2m} \geq r_m$	A_{sp}	0
21	$1 + r_p > z_{\text{sp}} > 1 - r_p$ $r_p + r_m > z_{\text{pm}} > r_p - r_m$ $1 + r_m > z_{\text{sm}} > 1 - r_m$ $l_{1s} \geq l_{2s} \geq 1$ $l_{1p} \geq l_{2p} \geq r_p$ $r_m \geq l_{1m} \geq l_{2m}$	A_{sp}	$A_{\text{sm}} - A_{\text{sp}}$
22	$1 + r_p > z_{\text{sp}} > 1 - r_p$ $r_p + r_m > z_{\text{sp}} > r_p - r_m$ $1 + r_m > z_{\text{sm}} > 1 - r_m$ $1 \geq l_{1s} \geq l_{2s}$ $l_{1p} \geq l_{2p} \geq r_p$ $r_m \geq l_{1m} \geq l_{2m}$	A_{sp}	$A_{\text{sm}} - A_{\text{pm}} + (A_p - A_{\text{sp}})$

Note. A_{op} and A_{om} are the areas of the stellar disk occulted by the planet and the moon respectively.

planet, and the moon, (see Figure 4) can be written as

$$A_{\text{spm1}} = A_{\Delta} + A_{\text{sa}} + A_{\text{pa}} + A_{\text{ma1}} \quad (29)$$

when $D \geq 0$. Otherwise,

$$A_{\text{spm2}} = A_{\Delta} + A_{\text{sa}} + A_{\text{pa}} + A_{\text{ma2}}, \quad (30)$$

where,

$$D = (c_{\text{mx}} - c_{\text{pmx}})(c_{\text{smy}} - c_{\text{pmy}}) - (c_{\text{my}} - c_{\text{pmy}})(c_{\text{smx}} - c_{\text{pmx}}), \quad (31)$$

which determines whether more than half of the moon is within the arc area (see Figure 4).

In the following expressions,

$$A_{\Delta} = \sqrt{s(s - s_{\text{sp}})(s - s_{\text{pm}})(s - s_{\text{sm}})}, \quad (32)$$

$$A_{\text{sa}} = \sin^{-1} \frac{s_{\text{pm}}}{2} - \frac{s_{\text{pm}}}{4} \sqrt{4 - s_{\text{pm}}^2}, \quad (33)$$

$$A_{\text{pa}} = r_p^2 \sin^{-1} \frac{s_{\text{sm}}}{2r_p} - \frac{s_{\text{sm}}}{4} \sqrt{4r_p^2 - s_{\text{sm}}^2}, \quad (34)$$

$$A_{\text{ma1}} = r_m^2 \sin^{-1} \frac{s_{\text{sp}}}{2r_m} - \frac{s_{\text{sp}}}{4} \sqrt{4r_m^2 - s_{\text{sp}}^2}, \quad (35)$$

$$A_{\text{ma}2} = r_m^2 \sin^{-1} \frac{s_{\text{sp}}}{2r_m} + \frac{s_{\text{sp}}}{4} \sqrt{4r_m^2 - s_{\text{sp}}^2}, \quad (36)$$

$$s_{\text{sp}} = \sqrt{(c_{\text{smx}} - c_{\text{pmx}})^2 + (c_{\text{smy}} - c_{\text{pmy}})^2}, \quad (37)$$

$$s_{\text{pm}} = \sqrt{(c_{\text{spx}} - c_{\text{smx}})^2 + (c_{\text{spy}} - c_{\text{smy}})^2}, \quad (38)$$

$$s_{\text{sm}} = \sqrt{(c_{\text{spx}} - c_{\text{pmx}})^2 + (c_{\text{spy}} - c_{\text{pmy}})^2}, \quad (39)$$

$$s = \frac{s_{\text{sp}} + s_{\text{pm}} + s_{\text{sm}}}{2}, \quad (40)$$

$$(c_{\text{mx}}, c_{\text{my}}) = (z_{\text{sm}} \cos \delta_{\text{sm}}, -z_{\text{sm}} \sin \delta_{\text{sm}}), \quad (41)$$

$$\cos \delta_{\text{sm}} = \frac{z_{\text{sp}}^2 + z_{\text{sm}}^2 - z_{\text{pm}}^2}{2z_{\text{sp}}z_{\text{sm}}}, \quad (42)$$

$$(c_{\text{spx}}, c_{\text{spy}}) = \left[\frac{1 - r_p^2 + z_{\text{sp}}^2}{2z_{\text{sp}}}, -\sqrt{1 - \left(\frac{1 - r_p^2 + z_{\text{sp}}^2}{2z_{\text{sp}}} \right)^2} \right], \quad (43)$$

$$(c_{\text{smx}}, c_{\text{smy}}) = (c'_{\text{smx}} \cos \delta_{\text{sm}} + c'_{\text{smy}} \sin \delta_{\text{sm}}, -c'_{\text{smx}} \sin \delta_{\text{sm}} + c'_{\text{smy}} \cos \delta_{\text{sm}}), \quad (44)$$

$$(c'_{\text{smx}}, c'_{\text{smy}}) = \left[\frac{1 - r_m^2 + z_{\text{sm}}^2}{2z_{\text{sm}}}, \sqrt{1 - \left(\frac{1 - r_m^2 + z_{\text{sm}}^2}{2z_{\text{sm}}} \right)^2} \right], \quad (45)$$

$$(c_{\text{pmx}}, c_{\text{pmy}}) = (-c''_{\text{pmx}} \cos \delta_{\text{pm}} + c''_{\text{pmy}} \sin \delta_{\text{pm}}, -z_{\text{sp}}, -c''_{\text{pmx}} \sin \delta_{\text{pm}} + c''_{\text{pmy}} \cos \delta_{\text{pm}}), \quad (46)$$

$$(c''_{\text{pmx}}, c''_{\text{pmy}}) = \left[\frac{r_p - r_m^2 + z_{\text{pm}}^2}{2z_{\text{pm}}}, -\sqrt{r_p^2 - \left(\frac{r_p - r_m^2 + z_{\text{pm}}^2}{2z_{\text{pm}}} \right)^2} \right], \quad (47)$$

and

$$\cos \delta_{\text{pm}} = \frac{z_{\text{sp}}^2 + z_{\text{pm}}^2 - z_{\text{sm}}^2}{2z_{\text{sp}}z_{\text{pm}}}. \quad (48)$$

Here, A_{Δ} is the area of the triangle and A_{sa} , A_{pa} , $A_{\text{ma}1}$, and $A_{\text{ma}2}$ are the areas of the arcs within the area of intersection of the three bodies (i.e., the star, the planet, and the moon); c_{sp} , c_{pm} , and c_{sm} are the coordinates of intersection of the three bodies; and c_m is the coordinate of the center of the moon.

3. Results and Discussion

The model parameters in the present formalism are r_p , r_m , t_{0b} , t_{0m} , P_b , P_m , r_{pm} , M_p/M_m , i_b , i_m , α_{mb} , and the limb-darkening coefficients of the host star defining $I(\rho)$, where all the distances are in terms of stellar radius. Here we have used the quadratic limb-darkening formula (Claret & Gimenez 1990; Claret 2000), given by

$$I(\rho)/I(0) = 1 - u_1(1 - \mu) - u_2(1 - \mu)^2, \quad (49)$$

where $\mu = \sqrt{1 - \rho^2}$, and u_1 and u_2 are the quadratic limb-darkening coefficients.

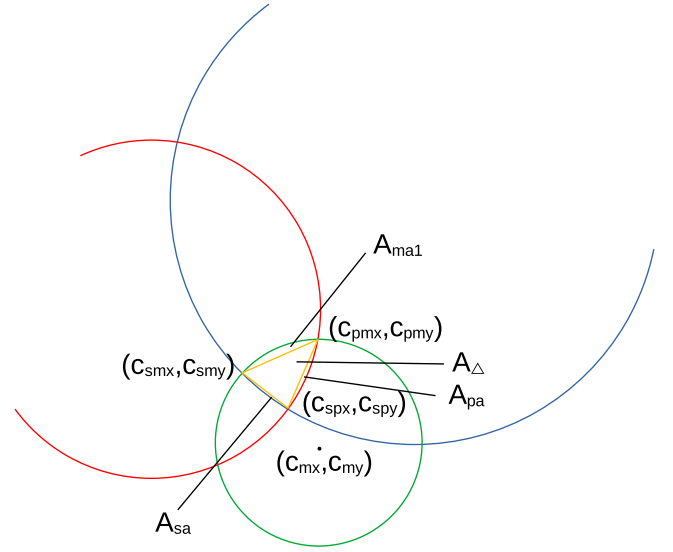


Figure 4. Alignment with intersection of all the three bodies (i.e., the star, the planet, and the moon) showing A_{Δ} , the area of the triangle, and A_{sa} , A_{pa} , and $A_{\text{ma}1}$, the areas of the arcs within the common area of intersection of the three bodies.

While generating the model transit light curves, we have used the analytical quadratic limb-darkening formalism for transit flux given by Mandel & Agol (2002). In the absence of such an analytical quadratic limb-darkening formula, we have used the small-body approximation to estimate the transit flux for the cases where all the three circular bodies overlap (see Section 2).

Let us now consider a scenario with $r_p = 0.1$, $r_m = 0.01$, $t_{0b} = 5$ days, $t_{0m} = 10$ days, $P_b = 300$ days, $P_m = 20$ days, $r_{\text{pm}} = 200$, $M_p/M_m = 1411$, $i_b = 90^\circ$, $i_m = 90^\circ$, $\alpha_{\text{mb}} = 0^\circ$, $u_1 = 0.4$, and $u_2 = 0.25$. Clearly, $i_b = i_m = 90^\circ$ implies that both the planet and the moon are transiting through the center of the star, and that combined with $\alpha_{\text{mb}} = 0^\circ$ implies that the orbit of the moon is aligned with the orbit of the planet, i.e., both the planet and the moon are in the same orbital plane. The transit light curve for this scenario is shown in Figure 5(a). Usually, the transit of the moon can take place before, during, or after the transit of the planet depending upon a combination of various parameters. For this scenario, we can see that the transit of the moon starts after the end of the planet's transit, as the moon is placed in a wide orbit around the planet, and its position makes it highly trailing while transiting the star. If we change the position of the moon by replacing $t_{0m} = 8$ days, as shown in Figure 5(b), we can see that the transit of the moon starts before the end of the transit of the planet.

The alignment of the orbit of an exomoon depends upon the formation and evolution path it followed. If the moon is formed from the circumplanetary disk, there is a higher probability for its orbit to be equatorial and it might be coaligned (coplanar) with the planetary orbit (Peale 1999). On the other hand, if the moon is formed through planetary capture or collision, its orbit may not be coaligned with the orbit of the planet. Both these situations can easily be modeled by using our formalism. When $i_b = i_m$ and $\alpha_{\text{mb}} = 0$, the orbits are coaligned. On the contrary, when $i_b \neq i_m$ and/or $\alpha_{\text{mb}} \neq 0$, the orbits are no longer coaligned with each other. To demonstrate it, let's consider a scenario by replacing $\alpha_{\text{mb}} = 20^\circ$ in the first scenario. As shown in Figure 6(a), we can see that both the transit depth and duration of the moon have decreased. This is because, in this case, the

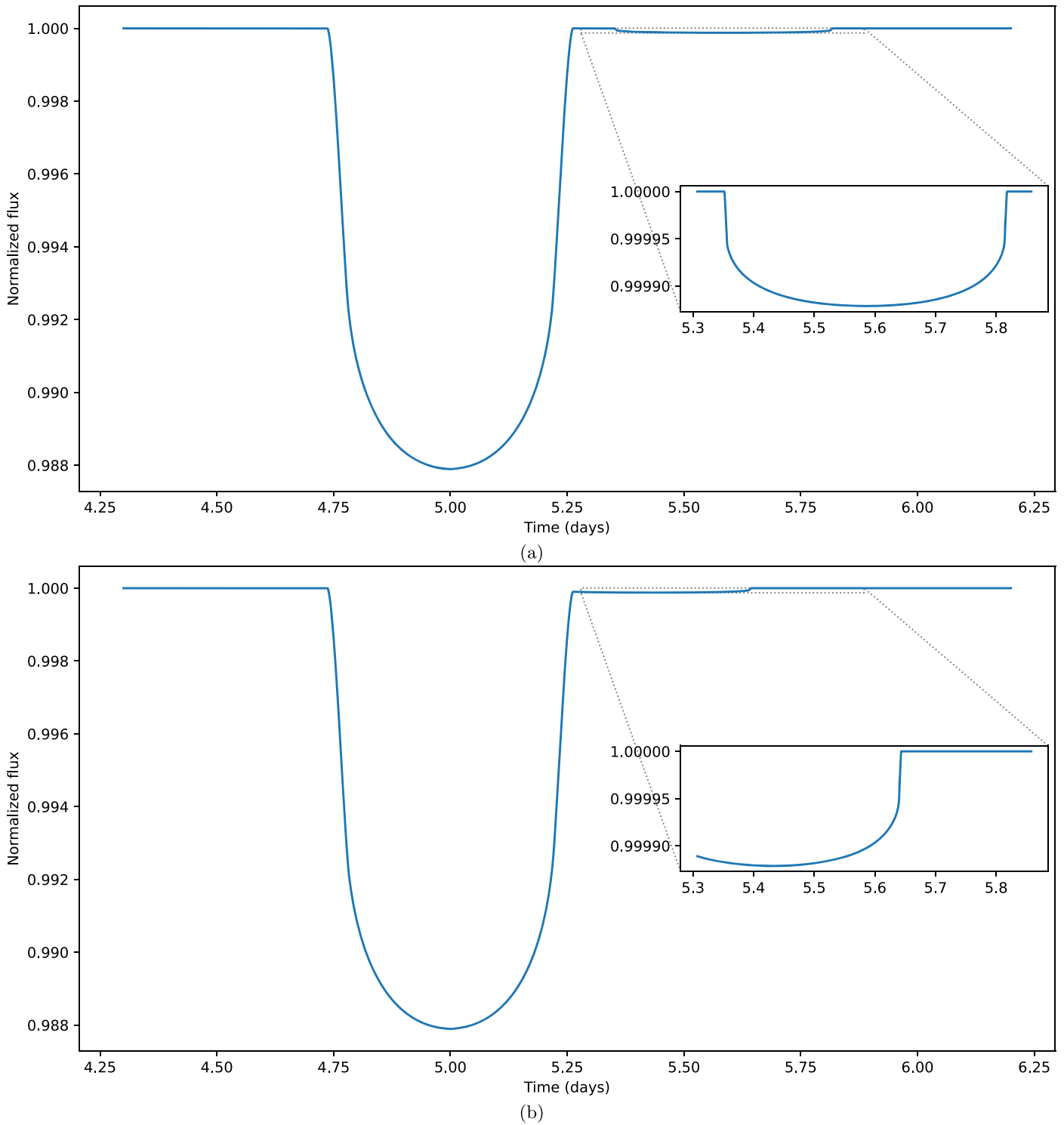


Figure 5. Transit light curves of a moon-hosting exoplanetary system: (a) with $r_p = 0.1$, $r_m = 0.01$, $t_{ob} = 5$ days, $t_{om} = 10$ days, $P_b = 300$ days, $P_m = 20$ days, $r_{pm} = 200$, $M_p/M_m = 1411$, $i_b = 90^\circ$, $i_m = 90^\circ$, $\alpha_{mb} = 0^\circ$, $u_1 = 0.4$, and $u_2 = 0.25$; (b) replacing $t_{om} = 8$ days.

moon is transiting toward the edge of the star instead of through the center as was in the case of the first scenario.

Obviously, if the moon is in a position such that it is fully transiting the planet or is fully eclipsed by it, while transiting the star, no transit signal due to the moon could be observed. Also, if the moon is in a wide and highly inclined orbit as compared to that of the planet, it may not transit the star every time the planet transits it (Martin et al. 2019). For example, if we replace $\alpha_{mb} = 30^\circ$ in the previous case, no transit is

observed for the moon. However, if the position of the moon is changed by replacing $t_{om} = 8$ days, the transit of the moon is observed as shown in Figure 6(b). Combining these factors along with the fact that exomoons are more likely to be found around planets in wider orbits around their host stars, i.e., planets with a much longer orbital period than a few days, it would require long period surveys continuously monitoring a particular portion of the sky to detect the exomoons. However, such surveys are also likely to increase the number of large

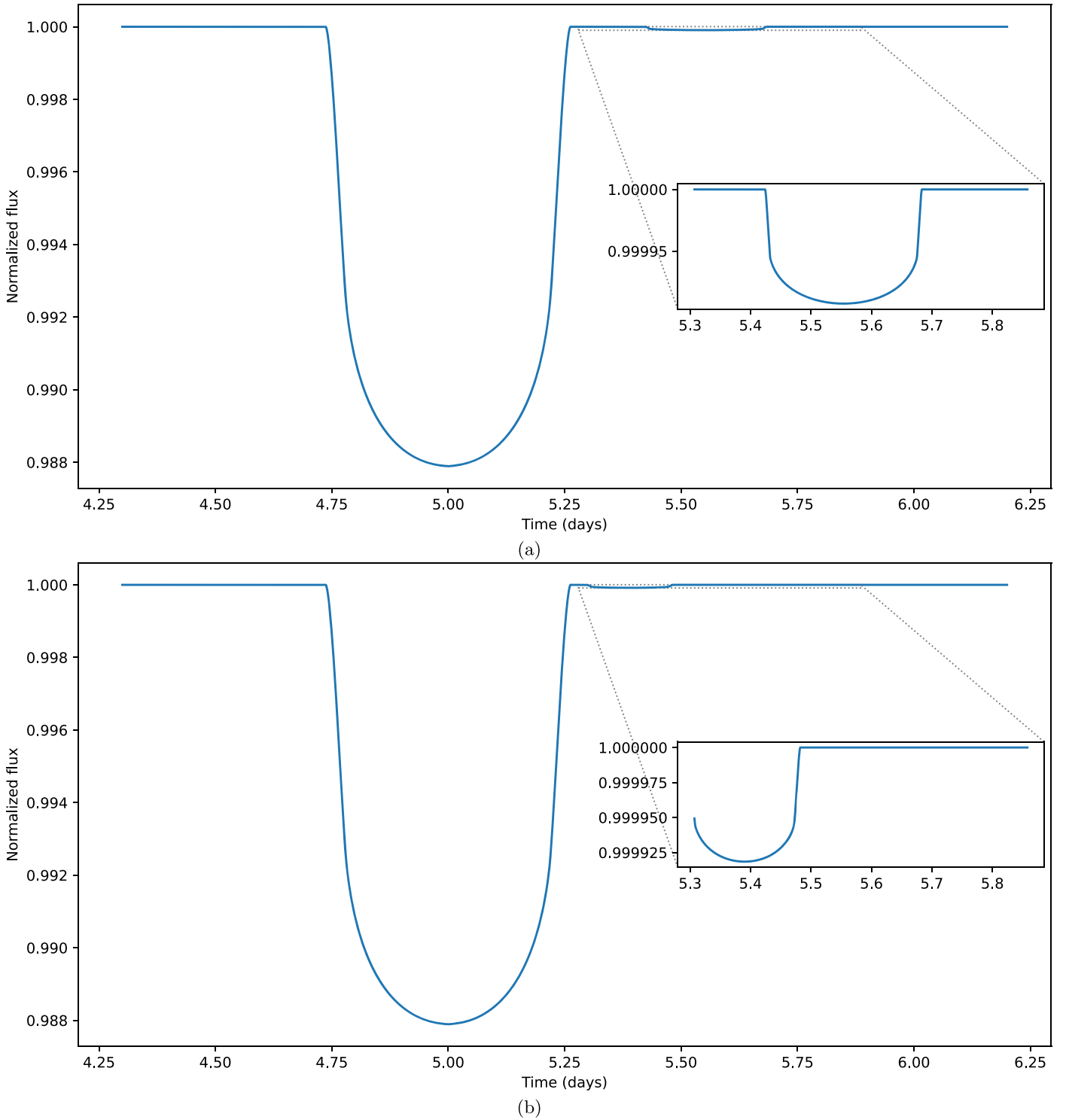


Figure 6. Transit light curves of a moon-hosting exoplanetary system: (a) with $r_p = 0.1$, $r_m = 0.01$, $t_{ob} = 5$ days, $t_{om} = 10$ days, $P_b = 300$ days, $P_m = 20$ days, $r_{pm} = 200$, $M_p/M_m = 1411$, $i_b = 90^\circ$, $i_m = 90^\circ$, $\alpha_{mb} = 20^\circ$, $u_1 = 0.4$, and $u_2 = 0.25$; (b) replacing $t_{om} = 8$ days and $\alpha_{mb} = 30^\circ$.

period exoplanets, including the habitable-zone terrestrial exoplanets, thereby increasing their effectiveness by detecting many interesting planetary- and subplanetary-mass bodies.

The photometric precision required to detect the exomoons is directly related to the transit depth, which is in turn dependent upon the ratio of disk area of the moon to that of the star. The required photometric precision is at a minimum for an exomoon in a system with a smaller M-dwarf-type star. Let us consider such a system with a moon the size of Earth’s Moon around a planet the

size of the Earth, i.e., $r_p = 0.075$, $r_m = 0.02$, $t_{ob} = 5$ days, $t_{om} = 10$ days, $P_b = 60$ days, $P_m = 15$ days, $r_{pm} = 25$, $M_p/M_m = 81$, $i_b = 90^\circ$, $i_m = 90^\circ$, $\alpha_{mb} = 0^\circ$, $u_1 = 0.4$, and $u_2 = 0.25$, the light curve for which is shown in Figure 7(a). If we change the position of the moon by replacing $t_{om} = 5$ days, there would arise a scenario where the moon transits the planet while simultaneously transiting the star as well. Such a scenario is presented in Figure 7(b).

To demonstrate the effect of the moon on the transit timing of the planet, we have coplotted the transit light curve of the

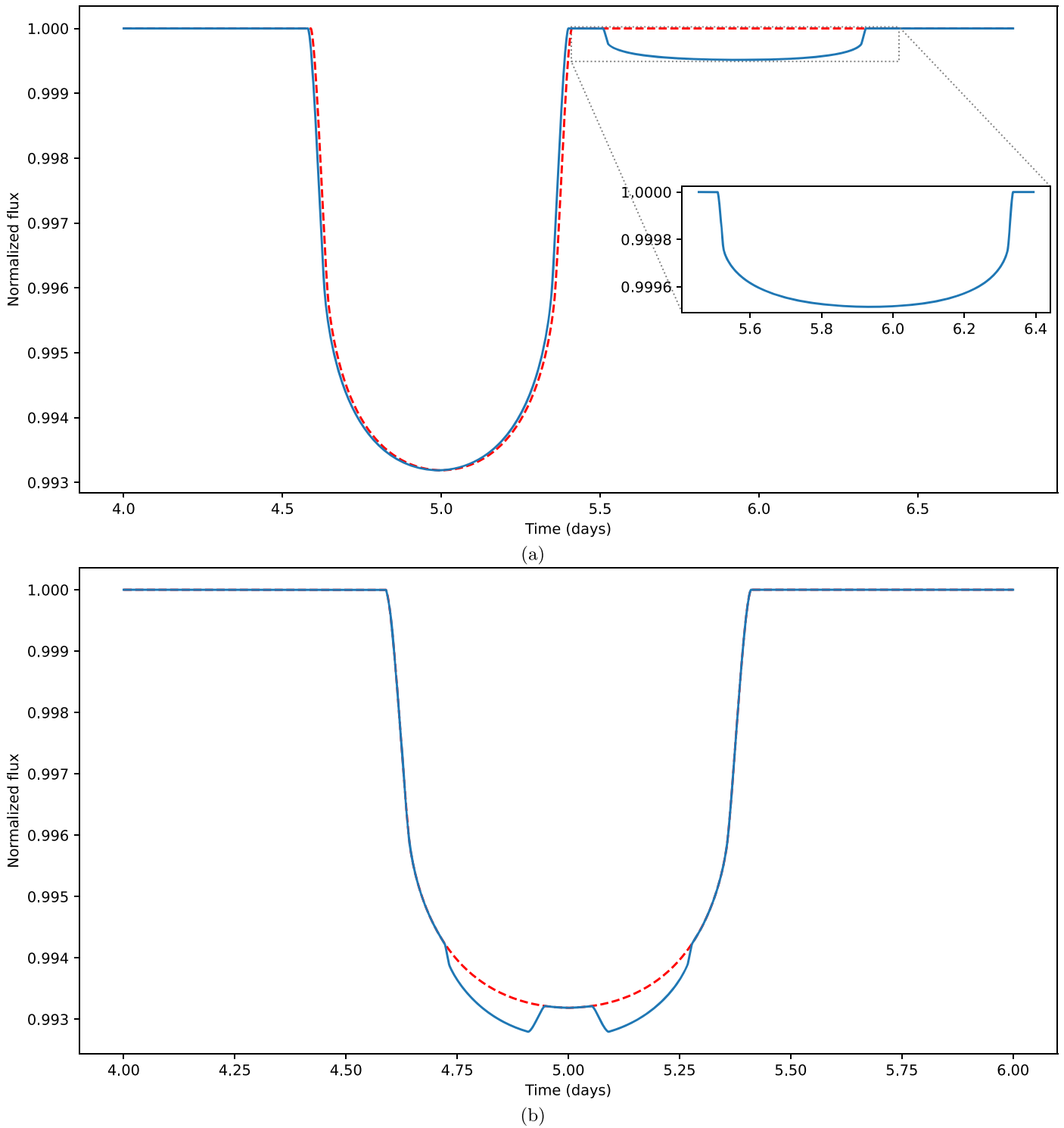


Figure 7. Transit light curves of a moon-hosting exoplanetary system: (a) with $r_p = 0.075$, $r_m = 0.02$, $t_{ob} = 5$ days, $t_{0m} = 10$ days, $P_b = 60$ days, $P_m = 15$ days, $r_{pm} = 25$, $M_p/M_m = 81$, $i_b = 90^\circ$, $i_m = 90^\circ$, $\alpha_{mb} = 0^\circ$, $u_1 = 0.4$, and $u_2 = 0.25$; (b) same but with $t_{0m} = 5$ days. The dashed red lines show the transit light curves of the planet in the absence of a moon. The TTV due to the presence of a moon can be observed in (a).

planet in the absence of a moon in Figure 7(a). Comparing the two light curves, the TTV can be observed. For a practical scenario, it could be difficult to detect the TTV in the observed transit data, as the barycentric offset from the center of the planet is quite small compared to the distance between the centers of the planet and the moon, even for a smaller mass

ratio between the planet and the moon (e.g., the earth–moon system, where $M_p/M_m \simeq 81$).

On the other hand, a higher precision would be required for systems with a larger host star. The minimum photometric precision required to detect a terrestrial exoplanet the size of the Earth around a star similar to the Sun is about 100 ppm (parts

per million). Therefore, a precision much better than that would be required to detect the exomoons around such systems. Such extremely high precision is expected to be achievable using the next generation of large telescopes, such as the James Webb Space Telescope (JWST), the European Extremely Large Telescope (E-ELT), the Thirty Meter Telescope (TMT), and the Giant Magellan Telescope (GMT), etc. Also, the instrumental and atmospheric noise effects have to be minimized for such observations. This can be achieved by using small-scale noise reduction techniques such as the wavelet denoising (Donoho & Johnstone 1994; Chakrabarty & Sengupta 2019; Saha et al. 2021; Saha & Sengupta 2021). The stellar variability and pulsations can also cause a challenge in such observations, which need to be reduced using techniques like the Gaussian process regression (Rasmussen & Williams 2006; Johnson et al. 2015; Chakrabarty & Sengupta 2019; Saha et al. 2021; Saha & Sengupta 2021).

4. Conclusion

In this paper, we have presented an analytical formalism to model the transit light curves for a system with a transiting exoplanet hosting an exomoon. The formalism uses the radius and orbital properties of both the planet and the moon as model parameters. The orbital alignment of the moon is taken with care by introducing two angular parameters and hence both the coaligned and noncoaligned orbit of a moon with respect to the planetary orbit can be modeled easily. This also enables us to model every possible scenario of alignment for the star–planet–moon system using this formalism.

The detection of exomoons requires extremely high precision observations, which are expected to be achievable using the next generation of very large telescopes along with the implementation of the existing critical noise reduction techniques. In such possibilities, our transit formalism could be useful to model the light curves in order to characterize the physical properties of the exomoons as well as to simulate every possible scenario and make strategies for such extremely time-critical observations.

We are thankful to the anonymous reviewer for a critical reading of the manuscript and for providing many useful comments and suggestions.

Appendix Derivation of l_{1s} and l_{2s}

From Figure 8, the angles γ_1 and γ_2 can be written as

$$\gamma_1 = \cos^{-1} \left(\frac{z_{sp}^2 + z_{pm}^2 - z_{sm}^2}{2z_{sp}z_{pm}} \right) \quad (\text{A1})$$

$$\gamma_2 = \cos^{-1} \left(\frac{r_p^2 - r_m^2 + z_{pm}^2}{2z_{pm}r_p} \right). \quad (\text{A2})$$

$$\begin{aligned} l_{1s} &= \sqrt{r_p^2 + z_{sp}^2 - 2r_pz_{sp} \cos(\gamma_1 + \gamma_2)} \\ &= \sqrt{r_p^2 + z_{sp}^2 - 2r_pz_{sp} \cos \left(\cos^{-1} \frac{z_{sp}^2 + z_{pm}^2 - z_{sm}^2}{2z_{sp}z_{pm}} + \cos^{-1} \frac{r_p^2 - r_m^2 + z_{pm}^2}{2z_{pm}r_p} \right)} \end{aligned} \quad (\text{A3})$$

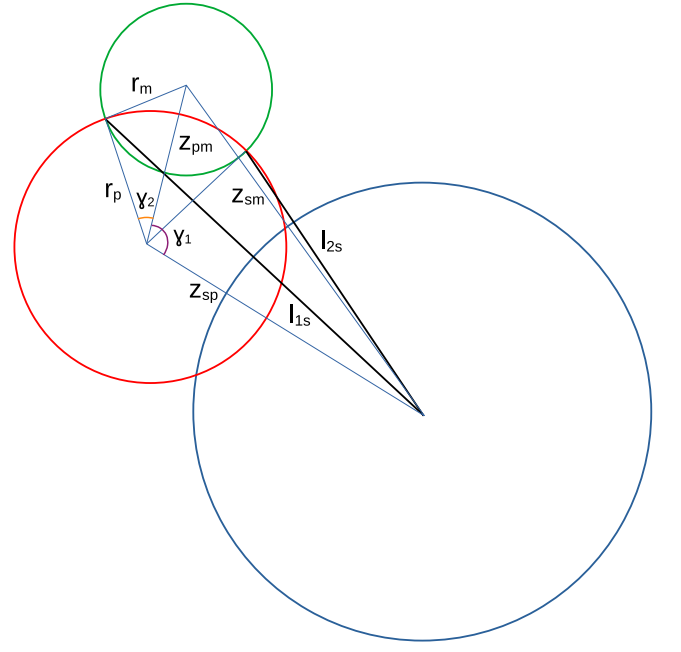


Figure 8. Alignment of the three bodies with star–planet and planet–moon intersections.

Now, l_{1s} and l_{2s} can be written as

$$\begin{aligned} l_{2s} &= \sqrt{r_p^2 + z_{sp}^2 - 2r_pz_{sp} \cos(\gamma_1 - \gamma_2)} \\ &= \sqrt{r_p^2 + z_{sp}^2 - 2r_pz_{sp} \cos \left(\cos^{-1} \frac{z_{sp}^2 + z_{pm}^2 - z_{sm}^2}{2z_{sp}z_{pm}} - \cos^{-1} \frac{r_p^2 - r_m^2 + z_{pm}^2}{2z_{pm}r_p} \right)}; \end{aligned} \quad (\text{A4})$$

l_{1p} , l_{2p} , l_{1m} , and l_{2m} can also be derived in a similar fashion.

ORCID iDs

Suman Saha  <https://orcid.org/0000-0001-8018-0264>
Sujan Sengupta  <https://orcid.org/0000-0002-6176-3816>

References

- Agol, E., Jansen, T., Lacy, B., Robinson, T. D., & Meadows, V. 2015, *ApJ*, **812**, 5
Cabrera, J., & Schneider, J. 2007, *A&A*, **464**, 1133
Chakrabarty, A., & Sengupta, S. 2019, *AJ*, **158**, 39
Claret, A. 2000, *A&A*, **363**, 1081
Claret, A., & Gimenez, A. 1990, *A&A*, **230**, 412
Dobos, V., Charoz, S., Pál, A., Roque-Bernard, A., & Szabó, G. M. 2021, *PASP*, **133**, 094401
Donoho, D., & Johnstone, I. 1994, *C. R. Acad. Sci.*, **319**, 1317
Fewell, M. P. 2006, Area of Common Overlap of Three Circles ADA463920, Defence Science and Technology Organisation Edinburgh (Australia) Maritime, <https://apps.dtic.mil/sti/citations/ADA463920>
Fox, C., & Wiegert, P. 2021, *MNRAS*, **501**, 2378
Han, C., & Han, W. 2002, *ApJ*, **580**, 490
Heller, R. 2014, *ApJ*, **787**, 14

- Johnson, M. C., Cochran, W. D., Collier Cameron, A., & Bayliss, D. 2015, *ApJL*, 810, L23
- Johnson, R. E., & Huggins, P. J. 2006, *PASP*, 118, 1136
- Kipping, D. 2020, *ApJL*, 900, L44
- Kipping, D. 2021, *MNRAS*, 500, 1851
- Kipping, D. M. 2009, *MNRAS*, 392, 181
- Kipping, D. M. 2011, *MNRAS*, 416, 689
- Lewis, K. M., Sackett, P. D., & Mardling, R. A. 2008, *ApJL*, 685, L153
- Livingston, J. H., Crossfield, I. J. M., Werner, M. W., et al. 2019, *AJ*, 157, 102
- Mandel, K., & Agol, E. 2002, *ApJL*, 580, L171
- Martin, D. V., Fabrycky, D. C., & Montet, B. T. 2019, *ApJL*, 875, L25
- Namouni, F. 2010, *ApJL*, 719, L145
- Noyola, J. P., Satyal, S., & Musielak, Z. E. 2014, *ApJ*, 791, 25
- Noyola, J. P., Satyal, S., & Musielak, Z. E. 2016, *ApJ*, 821, 97
- Oza, A. V., Johnson, R. E., Lellouch, E., et al. 2019, *ApJ*, 885, 168
- Peale, S. J. 1999, *ARA&A*, 37, 533
- Rasmussen, C. E., & Williams, C. K. I. 2006, *Gaussian Processes for Machine Learning* (Cambridge, MA: MIT Press)
- Saha, S., Chakrabarty, A., & Sengupta, S. 2021, *AJ*, 162, 18
- Saha, S., & Sengupta, S. 2021, *AJ*, 162, 221
- Sartoretti, P., & Schneider, J. 1999, *A&AS*, 134, 553
- Sengupta, S., & Marley, M. S. 2016, *ApJ*, 824, 76
- Spalding, C., Batygin, K., & Adams, F. C. 2016, *ApJ*, 817, 18
- Szabó, G. M., Sztatmáry, K., Divéki, Z., & Simon, A. 2006, *A&A*, 450, 395
- Teachey, A., & Kipping, D. M. 2018, *SciA*, 4, eaav1784
- Teachey, A., Kipping, D. M., & Schmitt, A. R. 2018, *AJ*, 155, 36
- Williams, D. M., & Knacke, R. F. 2004, *AsBio*, 4, 400